

Preparation of controlled ZnO nanostructures and their optical properties

Jun Yang¹ · Yongqian Wang¹ · Junhan Kong¹ · Meihua Yu² · Hongyun Jin¹

Received: 11 December 2015 / Accepted: 14 March 2016 / Published online: 16 March 2016
© Springer Science+Business Media New York 2016

Abstract ZnO nanostructures were synthesized via a facile template-free chemical method. The effect of different zinc sources on the morphologies and properties of ZnO nanostructures has been investigated. FESEM, XRD, UV–Vis absorption spectra and PL spectra were used to characterize the as-synthesized ZnO nanostructures. It has been found that the distinct surface morphologies of ZnO nanostructures grown by using $\text{Zn}(\text{CH}_3\text{COO})_2 \cdot 2\text{H}_2\text{O}$, $\text{Zn}(\text{NO}_3)_2 \cdot 6\text{H}_2\text{O}$, $\text{ZnSO}_4 \cdot 7\text{H}_2\text{O}$ and ZnCl_2 as ZnO zinc sources. The XRD patterns indicate that all the samples represent a hexagonal wurtzite structure and all diffraction peaks are indexed accordingly with the JCPDS card (No. 03-0888). The UV–Vis absorption spectra of them both exhibit a strong absorption in the ultraviolet region at band around at 400 nm. The band gaps of them are 3.17, 3.19, 3.20 and 3.27 eV, respectively. Being excited at 325 nm wavelength using a xenon lamp at room temperature, all the PL spectra consist of sharp emission in the UV range and abroad emission bands in the visible region ranging from 440 to 620 nm.

1 Introduction

Metal oxide (MOX) semiconductors play important roles in many areas of physics, chemistry biology and materials science [1]. Among the oxide semiconductors, ZnO is well-

known as a wide direct band gap ($E_g = 3.37$ at 300 K) semiconductors and possess wide application potentials in sensor [2–5], antibacterial activities [6], solar cells [7–9], optoelectronic [10], photocatalysis [11, 12], light emitting diodes (LED) [13] and so on. Control over the size, shape, surface roughness, and crystallization is of great significance for the fabrication of ZnO materials since they affect their performance in practical applications [14].

Up to now, a variety of methods such as magnetron sputtering [15], electrochemical deposition [16–19], chemical vapor deposition [20], sol–gel [21, 22], solvothermal synthesis [23] and hydrothermal method [24, 25] have been developed to prepare the ZnO structures. Over last few years, extensive efforts have been made on the synthesis of ZnO structures. Chemical route such as hydrothermal, sol–gel and aqueous solution [26] method have been widely used to synthesize ZnO nanostructures due to their morphology control, good stoichiometry control, easy scalability and low cost infrastructural requirements [27]. The main advantage of this method is the possibility to produce different type of high quality of structures in a simple way by using cheap aqueous systems. It is reported that a wide variety of morphologies of ZnO nanostructures have been prepared via chemical route, including ZnO spheres [28], nanowires [29], nanocapsules [30], nanotubes [31], nanorods [32].

Based on the above advantages, the ZnO nanostructures prepared by chemical method have shown much promise. In our work, ZnO nanostructures with new and interesting morphology of hexagonal rod structure had been achieved via chemical method by adding $(\text{CH}_3\text{COO})_2\text{Zn} \cdot 2\text{H}_2\text{O}$, $\text{Zn}(\text{NO}_3)_2 \cdot 6\text{H}_2\text{O}$, $\text{ZnSO}_4 \cdot 7\text{H}_2\text{O}$ or ZnCl_2 as zinc sources. And due to its multilayer structure, the ZnO nanostructures exhibited large surface area and enhanced lights capturing capacity. The highly ZnO structures with new and

✉ Yongqian Wang
cugwyq@126.com

¹ Faculty of Materials Science and Chemistry, China University of Geosciences, Wuhan 430074, China

² School of Materials Science and Engineering, Guangxi University, Nanning 530004, China

interesting morphology are expected to be widely applied in photocatalysis and optical device.

2 Experiment

2.1 Experimental procedure

All chemicals used in this work were of analytical reagent grade and used as received without further purification. All the aqueous solutions were prepared using deionized water. The ZnO nanostructures were obtained by a facile template-free chemical method. The ZnO nanostructures were obtained as follows: 2 M $(\text{CH}_3\text{COO})_2\text{Zn}\cdot 2\text{H}_2\text{O}$ was introduced into 4 M NaOH aqueous solution with the drop wise addition under continuous stirring in a magnetic stirrer at room temperature. Afterwards, the precipitate was filtrated, washed and dried at 60 °C for 8 h to obtain the $\text{Zn}(\text{OH})_2$ precursor. After that, 1.50 g of the $\text{Zn}(\text{OH})_2$ precursor was dispersed in 40 mL of 2 M NaOH aqueous solutions, then the white slurries were kept at 80 °C for 8 h and the final products were filtrated, washed with distilled water and absolute ethanol several times and then dried at 60 °C for 12 h. In order to obtain different samples for a clear comparison, $(\text{CH}_3\text{COO})_2\text{Zn}\cdot 2\text{H}_2\text{O}$ could be replaced with the $\text{Zn}(\text{NO}_3)_2\cdot 6\text{H}_2\text{O}$, $\text{ZnSO}_4\cdot 7\text{H}_2\text{O}$ or ZnCl_2 , while keeping other conditions intact.

2.2 Characterization

The morphology of the sample was characterized by using a field emission scanning electron microscope (FESEM) (SU8010, Hitachi). The crystal structure was measured by using an X-ray diffract meter (XRD) (D8 Advanced XRD, Bruker AXS). The UV–Vis absorption spectrum was measured by a UV–Vis spectrophotometer (UV-2550, Shimadzu, Japan). And the photo-luminescent (PL) spectrum of the sample was obtained using spectrophotometer at an excitation wavelength of 325 nm.

3 Results and discussion

3.1 FESEM images of ZnO nanostructures

Figure 1 shows the FESEM images of ZnO nanostructures grown by using $\text{Zn}(\text{CH}_3\text{COO})_2\cdot 2\text{H}_2\text{O}$, $\text{Zn}(\text{NO}_3)_2\cdot 6\text{H}_2\text{O}$, $\text{ZnSO}_4\cdot 7\text{H}_2\text{O}$ and ZnCl_2 as ZnO zinc sources. As shown in Fig. 1a, the smooth ZnO nanostructures was obtained by chemical method in $\text{Zn}(\text{CH}_3\text{COO})_2\cdot 2\text{H}_2\text{O}$ aqueous solution. The as-prepared nanostructures were rough and consisted of crystals with wide grain size distribution. Figure 1b also reveals the sheets structure of the ZnO

nanostructures. Besides, some regular structures with hexagonal sheet-shaped and novel structures such as flowers and cones can also be observed. Figure 1c reveals the structures with a uniform morphology, having a compact and densely accumulated appearance. Nevertheless, the ZnO nanostructures prepared in the aqueous solution of $\text{ZnSO}_4\cdot 7\text{H}_2\text{O}$ was uniform, and the spindles are of good shape, the spindles piled up together intensively, and presented abstract and ambiguous shape of flowers. Figure 1d reveals that the surface of the ZnO nanostructures obtained using ZnCl_2 possess a different morphology with hexagonal crystalline structure, and the sheets are more regular in shape with distinct edges and thinner than the other preparation condition.

3.2 XRD analysis

To study the crystallinity and crystal phase of the samples, X-ray diffraction analyses have been carried out. Figure 2 represents the XRD patterns of ZnO nanostructures synthesized by using $\text{Zn}(\text{CH}_3\text{COO})_2\cdot 2\text{H}_2\text{O}$, $\text{Zn}(\text{NO}_3)_2\cdot 6\text{H}_2\text{O}$, $\text{ZnSO}_4\cdot 7\text{H}_2\text{O}$ and ZnCl_2 as ZnO zinc sources. As seen in the obtained XRD patterns, peak positions match quite well with the wurtzite hexagonal and polycrystalline phase of ZnO (JCPDS No. 03-0888). The XRD patterns indicate that all the samples represent a hexagonal wurtzite structure and all diffraction peaks are indexed accordingly with the JCPDS card. Except ZnO, no other diffraction peak related to any impurity was detected in the XRD patterns, which indicate the high purity of the as prepared samples. Thus, the result shows that the ZnO nanostructures are hexagonal ZnO phase. All peaks are well resolved and quite sharp and it reveals that the crystallite size of ZnO is quite large. As shown in Fig. 2, the ZnO nanostructures have similar XRD patterns, with differences in their relative peak intensities due to their random orientation. The strong (101) and (002) diffraction peaks suggest that (101) and (002) are the preferred growth orientations of the ZnO nanostructures.

3.3 UV–Vis studies

Figure 3 exhibits the UV–Vis absorption spectra of ZnO nanostructures grown by using $\text{Zn}(\text{CH}_3\text{COO})_2\cdot 2\text{H}_2\text{O}$, $\text{Zn}(\text{NO}_3)_2\cdot 6\text{H}_2\text{O}$, $\text{ZnSO}_4\cdot 7\text{H}_2\text{O}$ and ZnCl_2 as zinc source. The as-synthesized ZnO nanostructures both possess excellent optical properties. The optical transmission of the ZnO nanostructures is very high in the visible range. It can be seen that the UV–Vis absorption spectra show a strong absorption in the ultraviolet region. As seen in Fig. 3, an obvious and significant absorption at wavelength less than 400 nm corresponds to the natural band gap absorption of the wurtzite hexagonal phase of ZnO. The absorption of ZnO nanostructures grown by using $\text{Zn}(\text{CH}_3\text{COO})_2\cdot 2\text{H}_2\text{O}$

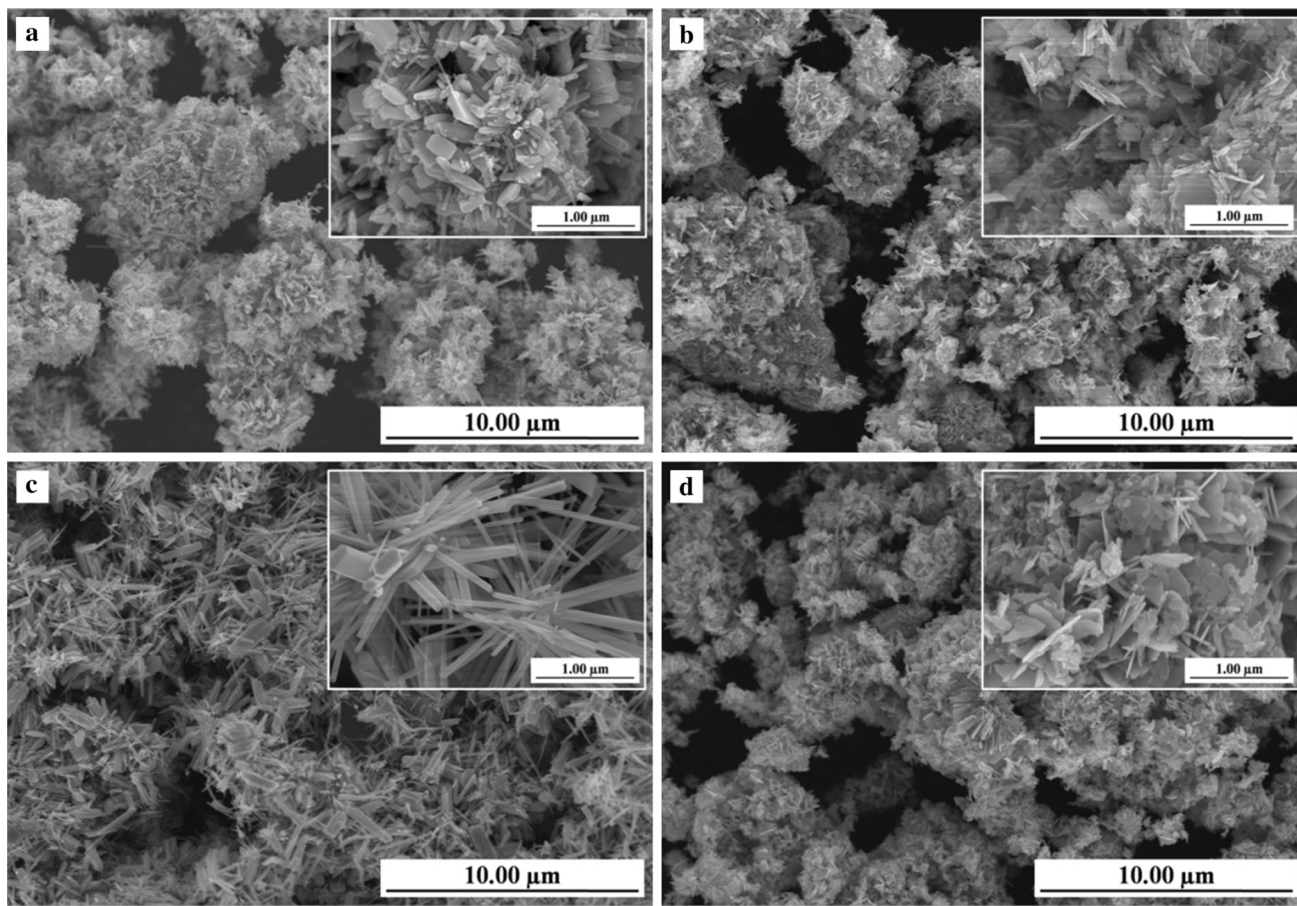


Fig. 1 FESEM images of ZnO nanostructures grown by using **a** $\text{Zn}(\text{CH}_3\text{COO})_2 \cdot 2\text{H}_2\text{O}$, **b** $\text{Zn}(\text{NO}_3)_2 \cdot 6\text{H}_2\text{O}$, **c** $\text{ZnSO}_4 \cdot 7\text{H}_2\text{O}$, **d** ZnCl_2

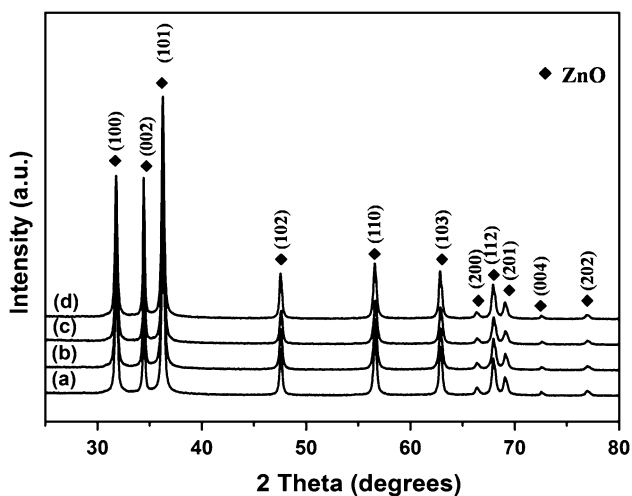


Fig. 2 XRD patterns of ZnO nanostructures grown by using **a** $\text{Zn}(\text{CH}_3\text{COO})_2 \cdot 2\text{H}_2\text{O}$, **b** $\text{Zn}(\text{NO}_3)_2 \cdot 6\text{H}_2\text{O}$, **c** $\text{ZnSO}_4 \cdot 7\text{H}_2\text{O}$, **d** ZnCl_2

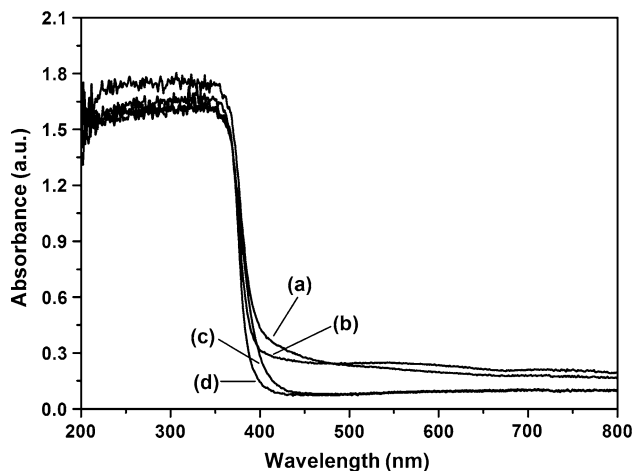


Fig. 3 UV-vis absorption spectra of ZnO nanostructures grown by using **a** $\text{Zn}(\text{CH}_3\text{COO})_2 \cdot 2\text{H}_2\text{O}$, **b** $\text{Zn}(\text{NO}_3)_2 \cdot 6\text{H}_2\text{O}$, **c** $\text{ZnSO}_4 \cdot 7\text{H}_2\text{O}$, **d** ZnCl_2

as zinc source in visible light region (380–700 nm) was enhanced dramatically, as shown in Fig. 3a. It is clearly seen that all the ZnO nanostructures exhibit an excitonic

absorption at band around at 400 nm. It is also noticeable that the ZnO nanostructures show a maximum absorption at 400 nm.

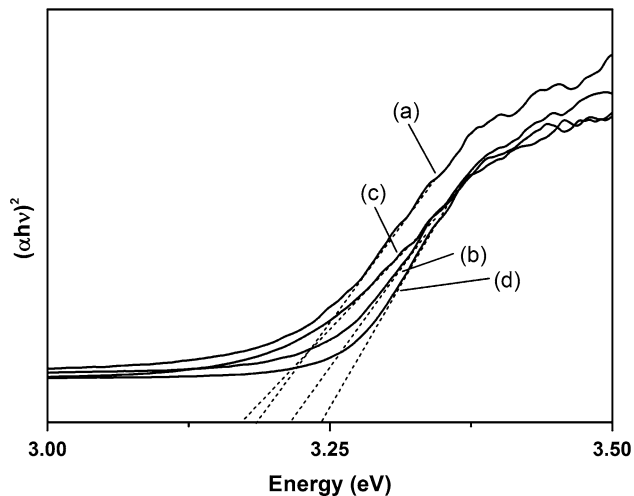


Fig. 4 $[\alpha hv]^2$ versus $h\nu$ plots of ZnO nanostructures grown by using **a** $\text{Zn}(\text{CH}_3\text{COO})_2 \cdot 2\text{H}_2\text{O}$, **b** $\text{Zn}(\text{NO}_3)_2 \cdot 6\text{H}_2\text{O}$, **c** $\text{ZnSO}_4 \cdot 7\text{H}_2\text{O}$, **d** ZnCl_2

Figure 4 shows the $[\alpha hv]^2$ versus $h\nu$ plots of ZnO nanostructures prepared using $\text{Zn}(\text{CH}_3\text{COO})_2 \cdot 2\text{H}_2\text{O}$, $\text{Zn}(\text{NO}_3)_2 \cdot 6\text{H}_2\text{O}$, $\text{ZnSO}_4 \cdot 7\text{H}_2\text{O}$ and ZnCl_2 as zinc sources. The optical band gap was derived based on the relationship of the absorption coefficient with incident photon energy $(\alpha hv) = B(h\nu - E_g)^n$, where α is the absorption coefficient, $h\nu$ is the energy of the incident photon, E_g is the band gap of semiconductor, n is $1/2$ for a direct transition semiconductor, e.g. ZnO. Since α is proportional to the absorbance values, the energy intercept of the curve of $[\alpha hv]^2$ versus $h\nu$ gives E_g when the linear region is extrapolated to the zero ordinate. The band gap of ZnO nanostructures grown by using $\text{Zn}(\text{CH}_3\text{COO})_2 \cdot 2\text{H}_2\text{O}$ as ZnO zinc source is further calculated to be 3.17 eV, the band gap of ZnO nanostructures grown by using $\text{Zn}(\text{NO}_3)_2 \cdot 6\text{H}_2\text{O}$ as ZnO zinc source is further calculated to be 3.19 eV, the band gap of ZnO nanostructures grown by using $\text{ZnSO}_4 \cdot 7\text{H}_2\text{O}$ as ZnO zinc source is further calculated to be 3.20 eV and the band gap of ZnO nanostructures grown by using ZnCl_2 as ZnO zinc source is further calculated to be 3.27 eV.

3.4 PL spectrum

Figure 5 exhibits the room temperature PL spectra in wavelengths ranging from the ultraviolet (UV) to the visible light region of ZnO nanostructures grown by using $\text{Zn}(\text{CH}_3\text{COO})_2 \cdot 2\text{H}_2\text{O}$, $\text{Zn}(\text{NO}_3)_2 \cdot 6\text{H}_2\text{O}$, $\text{ZnSO}_4 \cdot 7\text{H}_2\text{O}$ and ZnCl_2 as zinc source. All the PL spectra consist of sharp emission in the UV range and broad emission bands in the visible region ranging from 440 to 620 nm. These emission bands could be related to different emission centers of ZnO. It is obvious that the different zinc source significantly diminishes the PL intensity. A UV emission at wavelength of 400 nm coincides with UV–Vis absorption

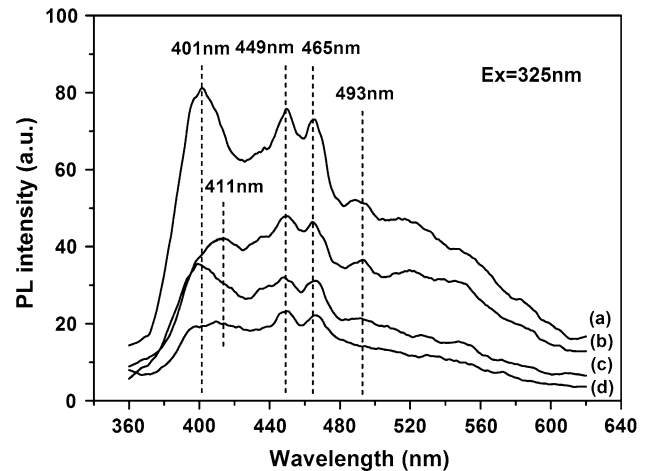


Fig. 5 PL spectra of ZnO nanostructures grown by using **a** $\text{Zn}(\text{CH}_3\text{COO})_2 \cdot 2\text{H}_2\text{O}$, **b** $\text{Zn}(\text{NO}_3)_2 \cdot 6\text{H}_2\text{O}$, **c** $\text{ZnSO}_4 \cdot 7\text{H}_2\text{O}$, **d** ZnCl_2

spectrum, which can be attributed to exciton emission, namely, the Auger recombination, which corresponding to near-band edge (NBE) transition. In Auger recombination processes, the energy released by an electron recombination is immediately absorbed by another electron, and then this energy is dissipated by phonons [15]. As a wide band gap material, Auger process depends on the concentration defects in the lattice. The origin of the emission peaks was analyzed according to the band structure and energy level of the defects in ZnO [33]. These visible emissions originate from their vacancies or defects that are located mainly on the emission centers of ZnO surface [30]. Therefore, surface state is the dominant factor that determines visible luminescence of ZnO. The emission peaks observed at 449 nm and 465 nm correspond to the interstitial oxygen (O_i), interstitial Zn (Zn_i) or transition between defects (interface traps) at grain boundaries and the valence band [25]. The weak blue emission peaks found at 493 nm could be attributed to the transition from antisite Zinc to O_i . The weak green emission bands observed at 520 nm possibly arise from the transition from conduction band bottom to Oxygen interstitial (O_i) [34]. It is clear that the wide UV emission is recorded for ZnO nanostructures grown by using $\text{Zn}(\text{CH}_3\text{COO})_2 \cdot 2\text{H}_2\text{O}$ as zinc source. We can also note that the UV emission is around at 411 nm. A slight red-shift of the emission compared to ZnO nanostructures grown by using other zinc source.

4 Conclusions

ZnO nanostructures were prepared using $\text{Zn}(\text{CH}_3\text{COO})_2 \cdot 2\text{H}_2\text{O}$, $\text{Zn}(\text{NO}_3)_2 \cdot 6\text{H}_2\text{O}$, $\text{ZnSO}_4 \cdot 7\text{H}_2\text{O}$ and ZnCl_2 as zinc sources by a template-free chemical method. The results show using different zinc sources have completely distinct

surface morphologies. The XRD patterns match well with the standard diffraction patterns, indicating the polycrystalline nature and hexagonal wurtzite structure of the samples. The UV–Vis absorption spectra of them both display an obvious and significant absorption at wavelength less than 400 nm. It can be seen that the UV–Vis absorption spectra show a strong absorption in the ultraviolet region. Meanwhile, the ZnO nanostructures prepared using $\text{Zn}(\text{NO}_3)_2 \cdot 6\text{H}_2\text{O}$ exhibit an outstanding visible light absorption. This behavior is mainly due to the high surface-to-volume ratio and higher content of oxygen vacancy. The room temperature PL spectra of ZnO nanostructures grown by different zinc sources possess a common feature that consists of a strong ultraviolet (UV) peak and visible emission band.

Acknowledgments This work was supported by the Fundamental Research Funds for National University (Nos. 1410491B04, 1510491B01), China University of Geosciences (Wuhan). The financial support was gratefully appreciated.

References

- D.E. Motaung, G.H. Mhlongo, S.S. Nkosi, G.F. Malgas, B.W. Mwakikunga, E. Coetsee, H.C. Swart, H.M.I. Abdallah, T. Moyo, S.S. Ray, Shape-selective dependence of room temperature ferromagnetism induced by hierarchical ZnO nanostructures. *ACS Appl. Mater. Interfaces* **6**, 8981–8995 (2014)
- X.H. Jiang, S.Y. Ma, W.Q. Li, T.T. Wang, W.X. Jin, J. Luo, L. Cheng, Y.Z. Mao, M. Zhang, Synthesis of hierarchical ZnO nanostructure assembled by nanorods and their performance for gas sensing. *Mater. Lett.* **142**, 299–303 (2015)
- M.L. Yin, S.Z. Liu, Controlled ZnO hierarchical structure for improved gas sensing performance. *Sensors Actuators B* **209**, 343–351 (2015)
- H.S. Al-Salman, M.J. Abdullah, Preparation of ZnO nanostructures by RF-magnetron sputtering on thermally oxidized porous silicon substrate for VOC sensing application. *Measurement* **59**, 248–257 (2015)
- S.H. Wei, J.H. Zhao, W.M. Du, Synthesis, characterization and acetone-sensing properties of bristlegrass-like ZnO nanostructure. *Ceram. Int.* **41**, 769–776 (2015)
- S. Shankar, X.N. Teng, G.B. Li, J.W. Rhim, Preparation, characterization and antimicrobial activity of gelatin/ZnO nanocomposite films. *Food Hydrocolloids* **45**, 264–271 (2015)
- C. Dunkel, M. Wark, T. Oekermann, R. Ostermann, B.M. Smarsly, Electrodeposition of zinc oxide on transparent conducting metal oxide nanofibers and its performance in dye sensitized solar cells. *Electrochim. Acta* **90**, 375–381 (2013)
- F.D. Nayeri, E.A. Soleimani, F. Salehi, Synthesis and characterization of ZnO nanowires grown on different seed layers: the application for dye-sensitized solar cells. *Renew Energy* **60**, 246–255 (2013)
- H.W. Choi, K.S. Lee, N.D. Theodore, T.L. Alford, Improved performance of ZnO nanostructured bulk heterojunction organic solar cells with nanowire-density modified by yttrium chloride introduction into solution. *Sol. Energy Mater. Sol. Cells* **117**, 273–278 (2013)
- A. Pruna, M.D. Reyes-Tolosa, D. Pullini, M.A. Hernandez-Fenollosa, D. Busquets-Mataix, Seed-free electrodeposition of ZnO bi-pods on electrophoretically-reduced graphene oxide for optoelectronic applications. *Ceram. Int.* **41**, 2381–2388 (2015)
- L.H. Yu, W. Chen, D.Z. Li, J.B. Wang, Y. Shao, M. He, P. Wang, X.Z. Zheng, Inhibition of photocorrosion and photoactivity enhancement for ZnO via specific hollow ZnO core/ZnS shell structure. *Appl. Catal. B* **164**, 453–461 (2015)
- J.F. Ma, K. Wang, L.Y. Li, T.L. Zhang, Y. Kong, S. Komarneni, Visible-light photocatalytic decolorization of Orange II on $\text{Cu}_2\text{O}/\text{ZnO}$ nanocomposites. *Ceram. Int.* **41**, 2050–2056 (2015)
- D.S. Yang, C. Lao, A.H. Zewail, 4D electron diffraction reveals correlated unidirectional behavior in zinc oxide nanowires. *Science* **321**(5896), 1660–1664 (2008)
- L.J. Zhang, X.M. Liu, C. Geng, H.J. Fang, Z.P. Lian, X.Q. Wang, D.Z. Shen, Q.F. Yan, Hexagonal crown-capped zinc oxide micro rods: hydrothermal growth and formation mechanism. *Inorg. Chem.* **52**, 10167–10175 (2013)
- Y. Liu, H.N. Liu, Y. Yu, Q. Wang, Y.L. Li, Z. Wang, Structural and optical properties of ZnO thin films with heavy Cu-doping prepared by magnetron co-sputtering. *Mater. Lett.* **143**, 319–321 (2015)
- W.T. Liang, W.P. Li, H.N. Chen, H.C. Liu, L.Q. Zhu, Exploiting electrodeposited flower-like $\text{Zn}_4(\text{OH})_6\text{SO}_4 \cdot 4\text{H}_2\text{O}$ nanosheets as precursor for porous ZnO nanosheets. *Electrochim. Acta* **156**, 171–178 (2015)
- J. Yang, X.F. Wang, T.T. Jiang, Y.C. Li, Q. Ma, J. Han, J.Y. Chen, J.X. Wang, Y.Q. Wang, Controllable preparation, growth mechanism and the properties research of ZnO nanocrystal. *Superlattices Microstruct.* **72**, 91–101 (2014)
- Y. Huang, D.K. Sarkar, X.G. Chen, Superhydrophobic nanostructured ZnO thin films on aluminum alloy substrates by electrophoretic deposition process. *Appl. Surf. Sci.* **327**, 327–334 (2015)
- J. Yang, Y.Q. Wang, T.T. Jiang, Y.C. Li, X.D. Yang, ZnO/ Er_2O_3 core-shell nanorod arrays: synthesis, properties and growth mechanism. *Appl. Surf. Sci.* **325**, 117–123 (2015)
- T. Hang, N.T. Dung, T.A. Truc, N.T. Duong, B.V. Truoc, P.G. Vu, T. Hoang, D. Thanh, M.G. Olivier, Effect of silane modified nano ZnO on UV degradation of polyurethane coatings. *Prog. Org. Coat.* **79**, 68–74 (2015)
- F. Boudjouan, A. Chelouche, T. Touam, D. Djouadi, S. Khodja, M. Tazerout, Y. Ouerdane, Z. Hadjoub, Effects of stabilizer ratio on photoluminescence properties of sol-gel ZnO nano-structured thin films. *J. Lumin.* **158**, 32–37 (2015)
- T. Georgakopoulos, N. Todorova, K. Pomoni, C. Trapalis, On the transient photoconductivity behavior of sol-gel TiO_2/ZnO composite thin films. *J. Non-Cryst. Solids* **410**, 135–141 (2015)
- G. Xu, X.L. Wang, G.Z. Liu, Facile solvothermal synthesis of abnormal growth of one-dimensional ZnO nanostructures by ring-opening reaction of polyvinylpyrrolidone. *Appl. Surf. Sci.* **329**, 137–142 (2015)
- J.P. Li, Q.F. Sun, C.D. Jin, J. Li, Comprehensive studies of the hydrothermal growth of ZnO nanocrystals on the surface of bamboo. *Ceram. Int.* **41**, 921–929 (2015)
- Y.Q. Wang, J. Yang, Y.C. Li, T.T. Jiang, J.Y. Chen, J.X. Wang, Controllable preparation of ZnO nanostructure using hydrothermal-electrodeposited method and its properties. *Mater. Chem. Phys.* **153**, 266–273 (2015)
- J. Wang, P.Y. Ma, L. Xiang, Effects of NaOH on formation of ZnO nanorods from $\epsilon\text{-Zn}(\text{OH})_2$. *Mater. Lett.* **141**, 118–121 (2015)
- X.G. San, G.S. Wang, B. Liang, Y.M. Song, S.Y. Gao, J.S. Zhang, F.L. Meng, Catalyst-free growth of one-dimensional ZnO nanostructures on SiO_2 substrate and in situ investigation of their H_2 sensing properties. *J. Alloy. Compd.* **622**, 73–78 (2015)
- P. Pandey, R. Kurchania, F.Z. Haque, Controlled hydrothermal synthesis, structural and optical analysis of nanometer-sized ZnO spheres. *Optik* **126**, 301–303 (2015)

29. R. Yousefi, A.K. Zak, Growth and characterization of ZnO nanowires grown on the Si (111) and Si (100) substrates: optical properties and biaxial stress of nanowires. *Mater. Sci. Semicond. Process.* **14**, 170–174 (2011)
30. M. Mouslmani, D. Patra, Modifying emission of ZnO nanoparticles in ZnO interceded polymer based hierarchical ordered nanocapsules. *Mater. Lett.* **143**, 135–139 (2015)
31. H. Lu, F. Zheng, M. Guo, M. Zhang, One-step electrodeposition of single-crystal ZnO nanotube arrays and their optical properties. *J. Alloy. Compd.* **588**, 217–221 (2014)
32. Y.Q. Wang, J. Yang, J.H. Kong, H.X. Jia, Z.S. Wang, H.Y. Jin, M.H. Yu, Synthesis of radial-like ZnO structure by hydrothermal method with $\text{ZnSO}_4 \cdot 7\text{H}_2\text{O}$ and $\text{Zn}(\text{CH}_3\text{COO})_2 \cdot 2\text{H}_2\text{O}$ as zinc sources. *Cryst. Res. Technol.* **50**, 414–419 (2015)
33. Ü. Özgür, Y.I. Alivov, C. Liu, A. Teke, M.A. Reshchikov, S. Doğan, V. Avrutin, S.J. Cho, H. Morkoç, A comprehensive review of ZnO materials and devices. *J. Appl. Phys.* **98**, 041301 (2005)
34. K. Vanheusden, W.L. Warren, C.H. Seager, D.R. Tallant, J.A. Voigt, B.E. Gnade, Mechanisms behind green photoluminescence in ZnO phosphor powders. *J. Appl. Phys.* **79**, 7983–7990 (1996)